A transformation from latency to ensemble coding in a model of piriform cortex

Merav Stern[1,2,4], Kevin A. Bolding[3], L.F. Abbott[2], Kevin M. Franks[3 *]

[1] Edmond and Lily Safra Center for Brain Sciences, Hebrew University, Jerusalem 9190401 Israel

[2] Department of Neuroscience, Zuckerman Mind Brain Behavior Institute, Columbia University, New York, New York 10027, USA

[3] Department of Neurobiology, Duke University School of Medicine, Durham, North Carolina 27705-4010, USA

[4] Present address: The Raymond and Beverly Sackler Scholars Program in Integrative Biophysics at the University of Washington, Seattle, Washington, 98195-3925, USA

* Correspondence: Kevin Franks
Bryan Research Building, Rm. 401D
311 Research Dr.
Durham, NC, 27705
(919) 684-3487
franks@neuro.duke.edu

Author contributions:
M.S., L.F.A. and K.M.F. conceived the project, performed and analyzed modeling studies, and wrote the manuscript with input from K.A.B.

Competing interests:
We have no financial or non-financial competing interests.

ABSTRACT

We present a spiking network model that transforms odor-dependent variable-latency olfactory bulb responses into a cortical ensemble code. In the model, which captures basic circuit properties of piriform cortex, the impact of the earliest-activated bulb inputs on the cortical response is amplified by diffuse recurrent collateral excitation, which then recruits strong feedback inhibition that stabilizes cortical activity and decreases the impact of later-responding glomeruli. Because the sequence of olfactory bulb activity for a particular odor is preserved across concentration, the ensemble of activated cortical neurons is robust to concentration changes. Nevertheless, odor concentration is represented by the latency and synchrony of the ensemble response. Using decoding techniques, we show that the ensemble-based coding scheme that arises in the cortical model supports concentration-invariant odor recognition.

12 **INTRODUCTION**

13 The coding schemes used to represent odors in the olfactory bulb and piriform cortex (PCx) are
14 different. In the bulb, odorants sequentially activate distinct subsets of glomeruli causing mitral
15 and tufted cells (MTCs) to begin firing at various odor- and cell-specific latencies following the
16 onset of inhalation (Spors and Grinvald 2002, Bozza et al. 2004, Bathellier et al. 2008, Carey et
17 al. 2009, Cury and Uchida 2010, Shusterman et al. 2011). In the PCx, this latency code is trans-
18 formed so that odors are represented by ensembles of neurons distributed across the piriform (Illig
19 and Haberly 2003, Rennaker et al. 2007, Poo and Isaacson 2009, Stettler and Axel 2009) with
20 spike timing providing little information about odor identity in the PCx (Miura et al. 2012, Uchida
21 et al. 2014) (see also Bolding & Franks, *submitted*). Here we construct a model, based on the circuit
22 architecture of PCx to explore the mechanisms that support the transformation from a bulbar la-
23 tency to a cortical ensemble odor code.

24

25 In mammals, odor perception begins when volatile molecules are inhaled and bind to odorant re-
26 ceptors expressed by olfactory sensory neurons (OSNs) in the nasal epithelium. Each OSN ex-
27 presses just one of ~1000 different odorant receptor genes, and all OSNs expressing a given re-
28 ceptor converge on a unique pair of glomeruli in the olfactory bulb (Wilson and Mainen 2006).
29 MTCs receive excitatory inputs from a single glomerulus, and their projections to PCx are diffuse
30 and overlapping (Ghosh et al. 2011, Miyamichi et al. 2011, Sosulski et al. 2011), allowing indi-
31 vidual pyramidal piriform neurons to receive inputs from different combinations of co-activated
32 glomeruli (Franks and Isaacson 2006, Suzuki and Bekkers 2006, Apicella et al. 2010, Davison and
33 Ehlers 2011). In addition to their connections onto pyramidal cells, MTCs make excitatory con-
34 nections onto layer 1 inhibitory interneurons that provide feedforward inhibition to pyramidal cells

(Luna and Schoppa 2008, Stokes and Isaacson 2010, Suzuki and Bekkers 2012). Pyramidal cells form a widespread recurrent collateral excitatory plexus that may amplify the effect of the earliest MTCs by recruiting additional pyramidal cells that initially receive slightly subthreshold bulb input (Franks et al. 2011). Recurrent excitation also recruits strong feedback inhibition from layer 3 interneurons that should, along with the feedforward inhibition, lessen the impact of later MTCs inputs (Franks et al. 2011, Suzuki and Bekkers 2012, Large et al. 2016). Piriform circuits are therefore poised to dramatically reshape odor representations (Davison and Ehlers 2011, Poo and Isaacson 2011, Haddad et al. 2013).

Although MTCs are activated at different times across the full respiration cycle (Bathellier et al. 2008, Cury and Uchida 2010, Shusterman et al. 2011), rodents can rapidly discriminate different odors within ~100 ms (Uchida and Mainen 2003, Abraham et al. 2004, Rinberg et al. 2006), well before most responsive glomeruli are activated (Wesson et al. 2008). Thus, the earliest activated glomeruli may provide most information about odor identity (Hopfield 1995, Schaefer and Margrie 2007, Schaefer and Margrie 2012, Wilson et al. 2015). Interestingly, most odors retain their perceptual identity across a range of concentrations (Krone et al. 2001, Laing et al. 2003, Homma et al. 2009). Note, however, that while increasing odor concentration systematically decreases MTCs onset latencies (Cang and Isaacson 2003, Margrie and Schaefer 2003, Spors et al. 2006, Junek et al. 2010, Gschwend et al. 2012) and can increase the total number of activated glomeruli, the sequences in which glomeruli are activated it preserved (Spors and Grinvald 2002, Junek et al. 2010). Thus, decoding the sequence in which glomeruli, and their associated MTCs, are activated has been hypothesized to provide a basis for concentration-invariant odor identification (Hopfield

1995, Junek et al. 2010, Schaefer and Margrie 2012, Wilson et al. 2015). Our model supports this hypothesis by providing a mechanism for its implementation in piriform cortex.

59 **RESULTS**

60 We use a modeling approach to provide mechanistic insight into how the transformation from the
61 latency code in the bulb to the ensemble code in PCx is implemented. We developed a spiking
62 network model that simulates patterns of odor-evoked mitral cell activity, and this provides input
63 to a spiking network mode that captures the specific circuit properties of PCx. We simulated bulb
64 and PCx spiking activity over the course of a single respiration cycle consisting of a 100 ms exha-
65 lation followed by a 200 ms inhalation.

66 Odors activate distinct ensembles of piriform neurons

67 Our model bulb consisted of 900 glomeruli that are each innervated by a unique family of 25 mitral
68 cells. Odor identities are defined by sets of glomerular onset latencies so that different odors acti-
69 vate specific subsets of glomeruli and their associated mitral cells with odor-specific latencies after
70 the onset of inhalation (Figure 1A, Supplemental Figure S1, and Methods). At our reference con-
71 centration, 10% of the glomeruli are activated during the 200 ms sniff.

72

73 The PCx model contains 10,000 excitatory pyramidal cells, each of which receives 50 excitatory
74 inputs from a random subset of the mitral cells and 1,000 recurrent excitatory inputs from a random
75 subset of other pyramidal cells (Figure 1B). Our model also includes 1,225 feedforward inhibitory
76 neurons that receive input from mitral cells and provide synaptic inhibition onto the pyramidal
77 cells and other feedforward interneurons, and a separate population of 1,225 feedback inhibitory
78 neurons that each receive inputs from a random subset of pyramidal cells and provide inhibitory
79 input locally onto pyramidal cells. We model all three classes of PCx neurons as leaky integrate-
80 and-fire neurons with current-based synaptic inputs (details and model parameter values are given

81

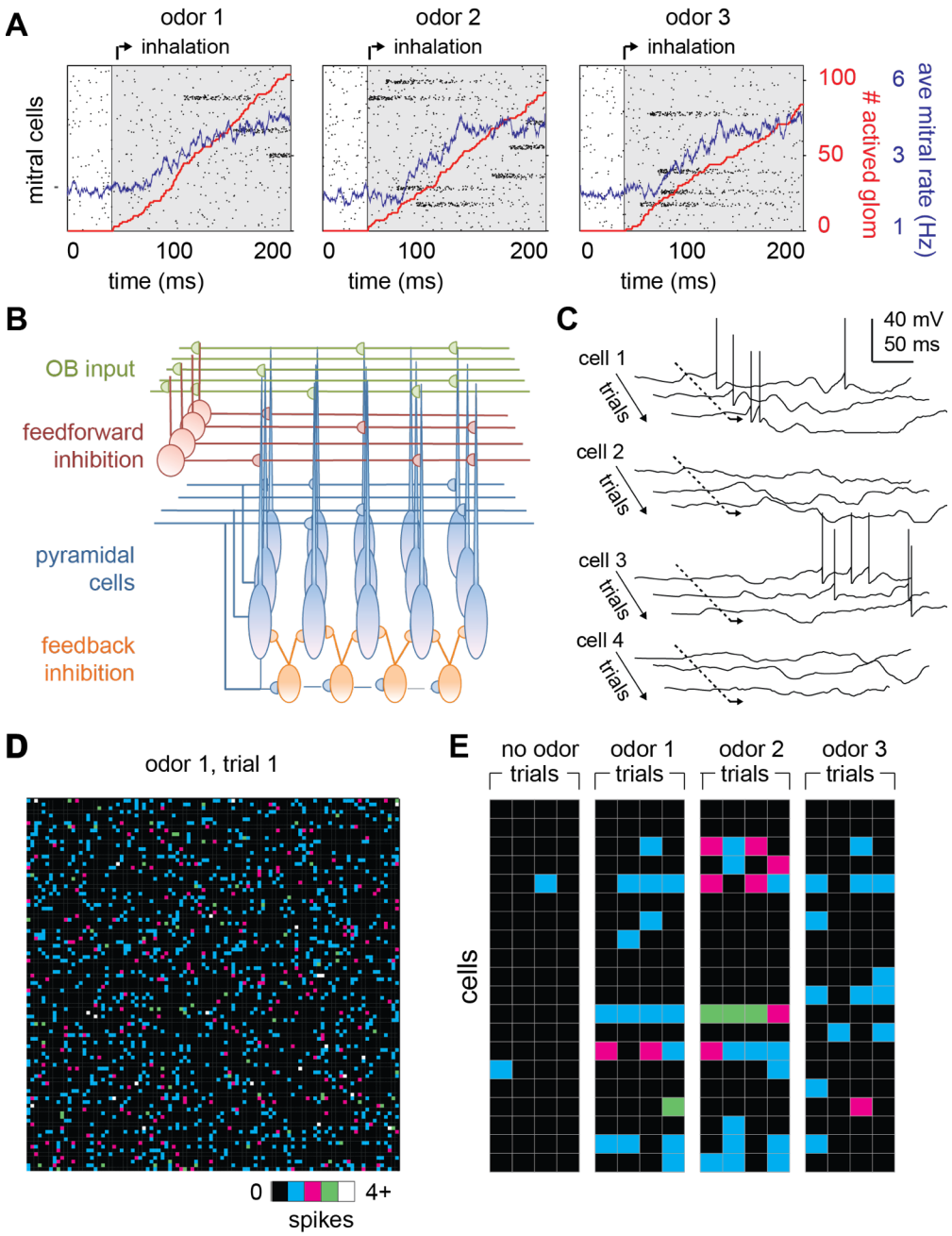

Figure 1. Odors activate distributed ensembles of PCx neurons.
(A) Raster plots showing spiking of 1,000 mitral cells (out of 22,500 total; 25 mitral cells/glomerulus, 40 glomeruli shown) in response to 3 different odors. Each row represents a single mitral cell and all mitral cells belonging to each glomerulus are clustered. Tick marks indicate spike times. Inhalation begins at 0 ms and is indicated by the grey shaded region. The red curve shows the cumulative number of glomeruli activated across the sniff, and the blue curve is the firing rate averaged across all mitral cells. (B) Schematic of the piriform cortex model. (C) Voltage traces for three sequential sniffs in 4 model pyramidal cells. Time of inhalation is indicated by the dashed line. (D) Single-trial population activity map for all 10,000 pyramidal cells. Each pixel represents a single cell, and pixel color indicates the number of spikes fired during the 200 ms inhalation. Approximately 13% of cells fired at least 1 action potential, with activated cells randomly distributed across the cortex. (E) Response vectors shown for 20 cells in response to different odors presented on 4 sequential trials. Spiking levels are low for no-odor controls. Note the trial-to-trial variability and that individual cells can be activated by different odors.

in the Methods). Most of our analyses focus on pyramidal cell activity because these cells receive bulb input and provide cortical output and thus carry the cortical odor code.

Low levels of spontaneous PCx spiking in the model are driven by baseline activity in mitral cells (1-2 Hz), with 2.8 ± 0.4 % (mean ± st. dev) of pyramidal cells spiking during the 200 ms inhalation in the absence of odor, consistent with experimental findings in awake (Zhan and Luo 2010, Miura et al. 2012) and anesthetized (Poo and Isaacson 2009) animals. Given this low level of spontaneous activity, cells that fire at least one action potential during the 200 ms inhalation are defined as "activated". Because each piriform cell receives input from a random subset of mitral cells, different odors selectively and specifically activate distinct, sparse subsets of cortical pyramidal cells (Figure 1C) so that each cell is responsive to multiple odors and each odor activates distinct ensembles of neurons distributed across PCx (Figure 1D,E). At our reference concentration, for which 10% of glomeruli are activated, 14.1 ± 0.59 % (mean ± st. dev., n = 6 odors) of piriform pyramidal cells fire at least one action potential during a sniff, which is also consistent with experimental data (Poo

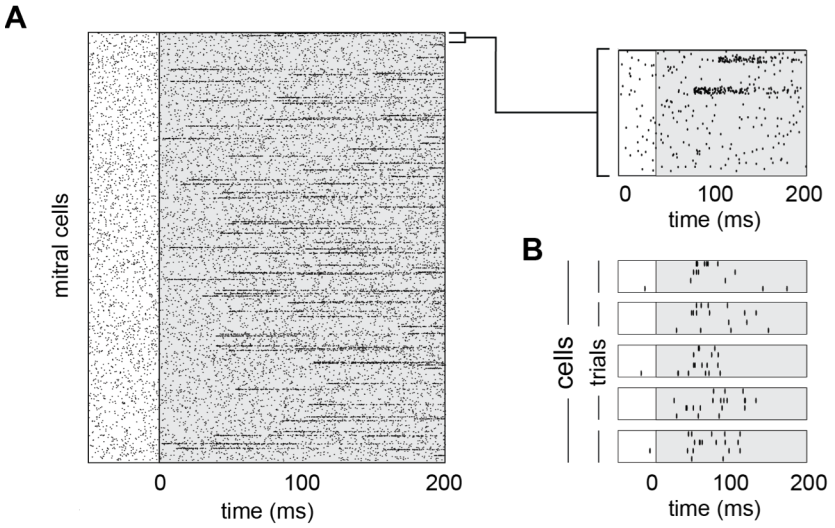

Supplementary Figure 1. Modeling odor responses in olfactory bulb
(A) Raster for all 22,500 mitral cells for one odor trial. Grey shading indicates inhalation phase. Inset shows expanded view of 1,000 mitral cells belonging to 40 different glomeruli. (B) Raster showing trial-to-trial variability for a single activated glomerulus. Each box represents a different sister mitral cell, with trials 1-4 represented by the lines within each box.

105 and Isaacson 2009, Stettler and Axel 2009, Miura et al. 2012). In summary, we have simulated
106 odor-evoked activity in olfactory bulb that we use as input to a model piriform cortex. Population
107 odor responses in the model broadly recapitulate experimental observations. We can therefore use
108 the model to probe how these population responses emerge mechanistically.

109 Evolution of cortical odor ensembles

110 We next illustrate how the model PCx ensembles evolve over time by comparing the spiking ac-
111 tivity of its four different classes of neurons (mitral cell, pyramidal cell, feedforward and feedback
112 inhibitory) over the course of a single sniff (Figure 2A). Preceding inhalation, baseline activity in
113 mitral cells drives low levels of spiking in both pyramidal cells and feedforward inhibitory neu-
114 rons. Feedback inhibitory neurons, which do not receive mitral cell input, show no baseline activ-
115 ity. Shortly after inhalation, inputs from the earliest activated glomeruli initiate a dynamic cascade
116 of cortical activity, characterized by a transient and rapid burst of spiking in a small subset of
117 pyramidal cells that is sharply truncated by the strong and synchronous recruitment of feedback
118 inhibitory neurons. The feedback inhibitory response suppresses pyramidal cell firing for a brief
119 period before the network settles into a sustained state with somewhat elevated pyramidal cell
120 activity that both drives and is held in check by feedback inhibition (Figure 2A). This activity
121 remains steady for the remainder of the inhalation, even though additional mitral cells respond,
122 because the activity of feedforward inhibitory neurons ramps up to cancel the increase in total
123 mitral cell input.

124

125 What triggers the rapid transient pyramidal cell response? Each odor initially activates a subset of
126 glomeruli that project randomly onto different cortical pyramidal cells. A small subset of pyrami-
127 dal cells receives enough input from short-latency mitral cells to reach threshold and start spiking

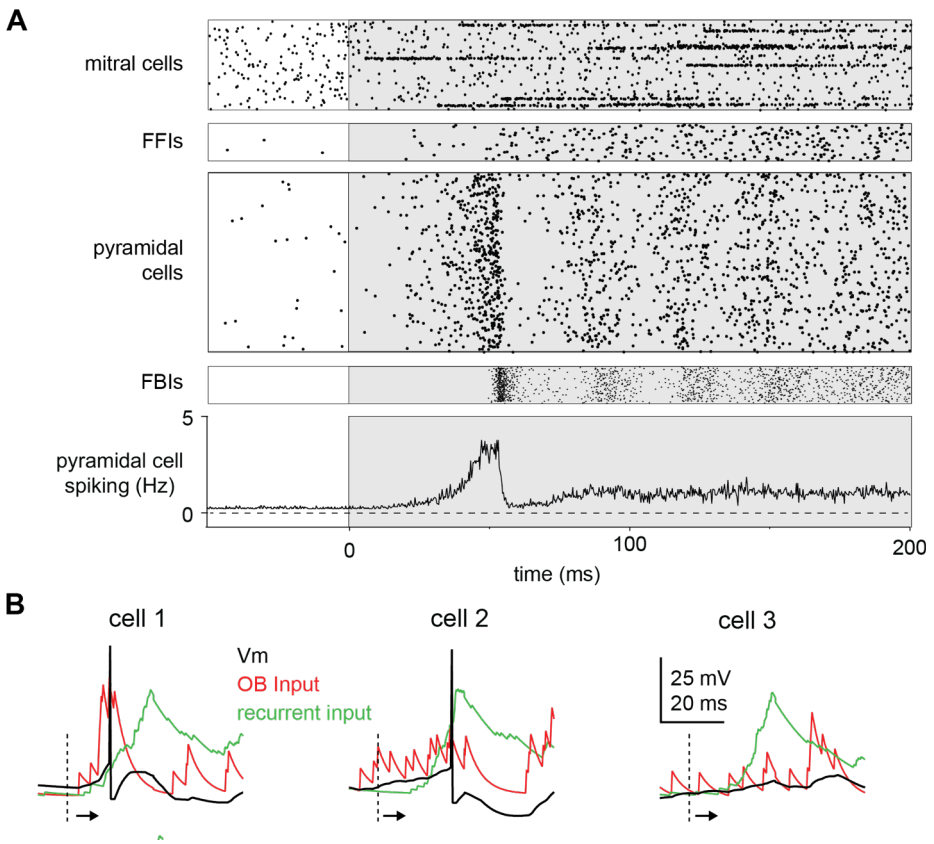

Figure 2. Evolution of a cortical odor response.
(A) Raster for a single sniff showing spiking activity of a subset of mitral cells (2,250 out of 22,500), all 1,225 feedforward interneurons (FFIs), all 10,000 pyramidal cells, and all 1,225 feedforward interneurons (FBIs). Spiking rate for the population of pyramidal cells is shown at the bottom (average of 6 trials). Note that the earliest activated glomeruli initiate a cascade of pyramidal cell spiking that peaks after ~50 ms and is abruptly truncated by synchronous spiking of FBIs. (B) Single-trial voltage traces (black) for 3 pyramidal cells in response to the same odor. Inhalation onset is indicated by the dashed line. The red traces show the bulb input and the green traces the recurrent input received by each cell. Cell 1 receives strong bulb input and spikes soon after odor presentation. Cell 2 receives subthreshold input from the bulb and only spikes after receiving addition recurrent input from other pyramidal cells. Cell 3 receives no early odor-evoked input from the bulb, and its recurrent input is subthreshold, so it does not spike over the time period shown.

early in the sniff (Figure 2B, cell 1). This activity produces a small amount of recurrent excitation that is dispersed across the cortex via the long-range recurrent collateral connections. The resulting recurrent input is not strong enough to drive spiking by itself (Figure 2B, cell 3), but it can recruit other pyramidal cells that receive moderate but subthreshold bulb input (Figure 2B, cell 2). Because more cells received subthreshold than suprathreshold bulb input, more pyramidal cells are activated by the recurrent input, resulting in even stronger recurrent excitation that, in turn, can

help activate even more pyramidal cells receiving even less bulb input. The result is an explosive increase in total pyramidal cell activity, and therefore a steady increase in the strength of recurrent excitation. However, recurrent excitation onto feedback inhibitory neurons is stronger than onto other pyramidal cells so that feedback inhibitory neurons are recruited before pyramidal cells that have not received any direct bulb input. Thus, feedback inhibition quickly halts the explosive growth of pyramidal cell firing because pure recurrent input always remains subthreshold for pyramidal cells, thereby maintaining the odor-specificity of the cortical ensemble.

Specific roles for different circuit elements in shaping cortical responses

To reveal the specific roles that different circuit elements play in shaping piriform output we compared responses in the full circuit with those obtained after removing different circuit elements (Figure 3). The same odor stimulus was used in all cases, so input from the olfactory bulb is identical except for the trial-to-trial stochasticity of mitral cell spiking. We first compared responses in the full circuit (Figure 3A) with those in a purely feedforward network in which pyramidal cells only receive mitral cell inputs (Figure 3B). In this highly reduced, feedforward circuit, pyramidal cell spiking activity grows more slowly, without any strong initial transient, and it tracks the number of spiking mitral cells. In the absence of either feedforward or feedback inhibition, the cortical response continues to grow over the course of the sniff as more glomeruli are activated (Figure 1A), so that a large fraction of cells respond at some point during the course of the entire sniff.

We next examined networks without feedforward or feedback inhibition, or without recurrent excitation and excitatory input to feedback interneurons. Eliminating only feedforward inhibition increases the amplitude of the peak pyramidal response by about 50%, although the general shape

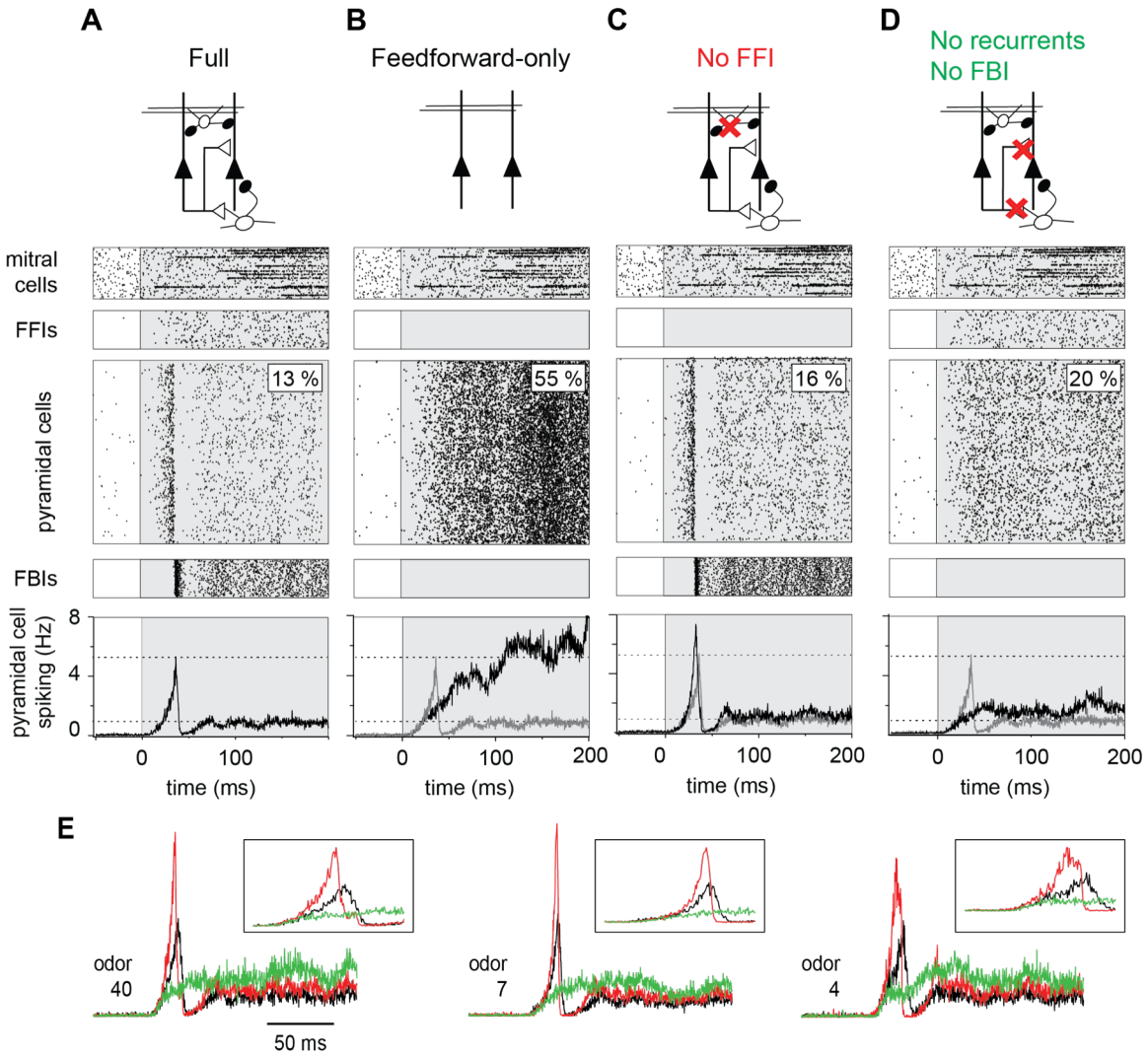

Figure 3. Distinct roles for different inputs in shaping ensemble response.
(A-D) Raster plots for presentations of the same odor using different circuit configurations. The percentages of active pyramidal cells are shown in the insets. (A) As in Figure 2A. (B) Network activity when pyramidal cells get excitatory input from mitral cells but without FFI, recurrent excitation or FBI. Pyramidal cell spiking tracks mitral cell input. Population rate for the full network is shown in grey for comparison. (C) Network activity after eliminating excitatory input to FFIs. Note that sustained FBI spiking increases without FFI, resulting in roughly constant levels of sustained spiking in pyramidal cells. (D) Network activity with no recurrent excitation onto either other pyramidal cells or FBIs. The transient activity peak seen in A-D is absent, and sustained activity is slightly higher. (E) Population rate plots for 3 different odors with the full network (black trace), no FFI (red trace) or no recurrent excitation/FBI (green trace). Insets expand the period around inhalation. Note the population spiking is higher and peaks slightly earlier without FFI, and that responses are slow without recurrent excitation. All population spike rate plots are averaged over 6 trials.

of the population response is largely unchanged (Figure 3C,E) and the fraction of cells activated over the entire sniff only increases modestly (from 13% to 16%). When we selectively eliminated feedback inhibition, odor induces unchecked runaway recurrent excitation, and all the cells end up

spiking vigorously (not shown). Finally, we simulated the circuit with pyramidal cell output blocked, which eliminates both recurrent excitation and the recruitment of feedback inhibition. Under these conditions pyramidal cell spiking initially ramps slowly, similar to the feedforward-only condition, but then plateaus within ~50 ms, as feedforward inhibition is recruited (Figure 3D,E). Although the rapid peak in instantaneous spiking activity is substantially decreased under these conditions, activity over the whole sniff increases, with 20% of the pyramidal cells responding. These results illustrate the istinct roles that different elements of the model PCx play in shaping odor responses.

Piriform responses are shaped by early-responding glomeruli

The previous analysis showed that population spiking peaks early when recurrent excitation is present (Figures 3A,C) but ramps up more slowly when it is eliminated (Figures 3B,D), indicating a key role for intracortical circuitry in amplifying the initial response. We examined this directly by comparing population spiking to the sequential activation of individual glomeruli (Figure 4A). In the full network, population spiking peaks 34 ± 8.3 ms after inhalation onset (mean ± st. dev. for 6 odors with ensemble averages of 6 trials per odor, at the reference concentration; Figure 4B,C). At this time, only 15 ± 1.4 glomeruli have been activated out of the 95 ± 6.0 glomeruli that will eventually be activated across the full sniff. In other words, at its peak, PCx activity is driven by the earliest ~15% of activated glomeruli. Mean responses peak slightly earlier when feedforward inhibition is eliminated (28 ± 4.5 ms; Figure 4B), but the peak activity is still driven by a similar number of glomeruli (12 ± 0.80 glomeruli; Figure 4C); on individual trials, the peak response is larger without feedforward inhibition (Figure 3C,D), but this difference is not captured

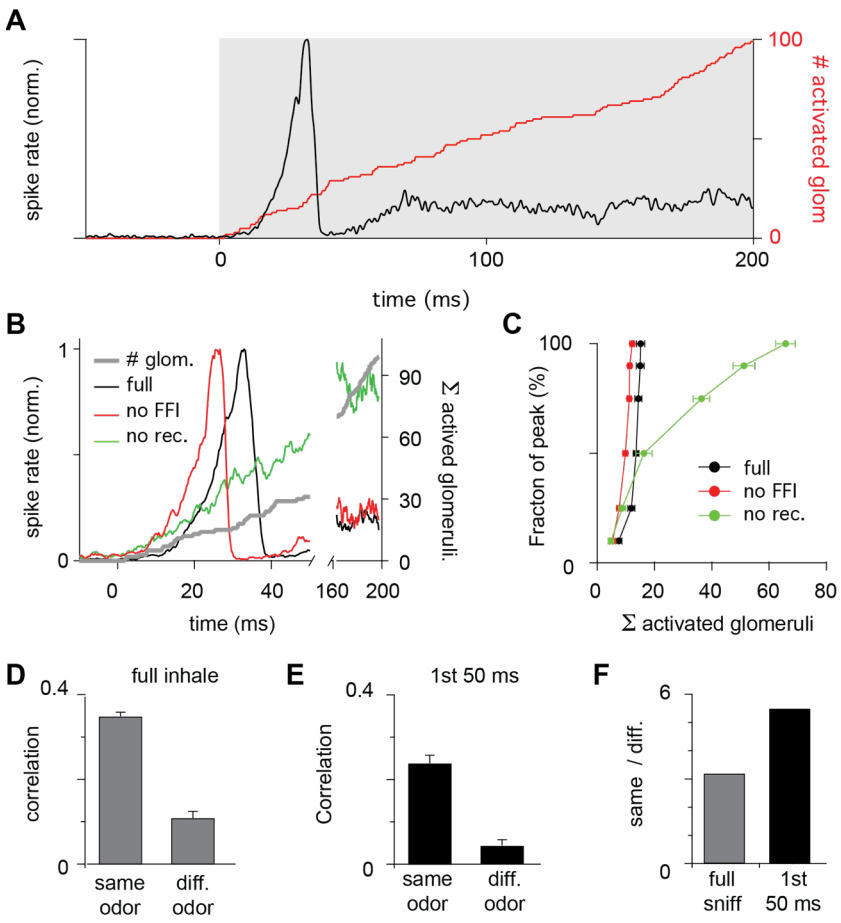

Figure 4. Earliest-active glomeruli define the cortical response.
(A) Normalized population spike rates (black) in response to an odor during the sniff cycle shown in grey. The red curve shows the cumulative number of glomeruli activated across the sniff. Note that population spiking peaks after only a small subset of glomeruli have been activated. (B) Normalized population spike rates for one odor for the full network (black trace), without FFI (red trace) and without recurrent excitation (green trace). Grey trace shows the cumulative number of activated glomeruli. (C) Fraction of peak population spike rate as a function of the cumulative number of activated glomeruli for 6 different odors. These curves indicate the central role recurrent excitation plays in amplifying the impact of early-responsive glomeruli. (D) Average correlation coefficients for repeated same-odor trials and pairs of different-odor trials measured over the full 200 ms inhalation. (E) As in D but measured over the first 50 ms after inhalation onset. (F) Ratios of correlations for same- vs. different-odor trials measured over the full sniff (grey bar on left) and over the first 50 ms (black bar on right).

in the average responses). In contrast, population spiking peaks much later without recurrent excitation (139 ± 29 ms) at a time when most of the responsive glomeruli have been activated (66 ± 0.44; Figure 4C). Recurrent excitation therefore plays an important role in shaping the dynamics

of the cortical odor response by amplifying the impact of early-responsive glomeruli and discounting the impact of later-responding glomeruli through the recruitment of strong feedback inhibition (Franks et al. 2011).

We wondered whether the earliest part of the cortical response provides a more distinctive representation of odor identity than the later response, so we quantified responses as vectors of spike counts, one component for each pyramidal cell, either over either the full 200 ms inhalation or only the first 50 ms after inhalation onset. We then compared pair-wise correlations between response vectors on either same-odor trials or trials involving different odors. Even though glomerulus onset latencies are identical in all same-odor trials, stochastic mitral cell firing results in considerable trial-to-trial variability (Figure 1E). Consequently, correlations coefficients are low for same-odor trial pairs over the full sniff (0.35 ± 0.010, mean ± st. dev. for multiple same-odor trial pairs using 6 different odors; Figure 4D). Nevertheless, same-odor responses are considerably more correlated than pairs of responses to different odors (0.11 ± 0.016; mean ± st. dev. for pairs of the same 6 odors). Response correlations to both same-odor and different-odor responses are lower when using only first 50 ms (same-odor, 0.24 ± 0.019; different-odor pairs, 0.044 ± 0.014; Figure 4E). However, the ratio of correlations for same- vs. different-odor responses, which can be thought of as a signal-to-noise ratio, is almost double in the first 50 ms versus the full 200 ms inhalation (Figure 4F). Taken together, our model predicts that a cascade of cortical activity is initiated by the earliest-responsive inputs and amplified by recurrent excitation, providing a distinctive odor representation, and then truncated by feedback inhibition. The cortical odor response is therefore largely shaped by the glomeruli that respond earliest in the sniff.

208 Distinct roles for feedforward and feedback inhibition in normalizing PCx output

209 We next asked how cortical odor representations depend on odor concentration. Onset latencies
210 decrease with increasing concentrations of odorant (Cang and Isaacson 2003, Junek et al. 2010,
211 Sirotin et al. 2015), which we simulate in our olfactory bulb model (Figure 5A) by shrinking the
212 onset latencies from those at the reference concentration. In other words, to decrease odor concen-
213 tration, we uniformly stretch latencies causing fewer glomeruli to be activated within 200 ms, and
214 making those that do activate respond later. Conversely, we shrink the set of latencies to simulated
215 higher concentrations so that glomeruli are activated earlier. Importantly, stretching or shrinking
216 latencies does not change the sequence in which glomeruli become activated (Figure 5A). We
217 quantify odor concentration using the fraction of activated glomeruli. Note that given the non-
218 linear concentration-dependence of receptor activation and extensive normalization at each multi-
219 ple stages of the system upstream of the cortex (Cleland et al. 2011), a 10-fold increase in mitral
220 cell output is expected to correspond to a much, much greater range of concentration.

221

222 The number of responsive pyramidal cells could scale with the total amount of glomerular input,
223 which increases at higher concentrations. However, PCx odor ensembles are buffered against
224 changes in odor concentration (Figure 5B). Across the population, we found that the number of
225 responsive pyramidal cells only increases by 50% upon a 10-fold increase in input (Figure 5C).
226 This indicates that the size of cortical odor ensembles is only weakly concentration-dependent,
227 consistent with in vivo imaging studies (Stettler and Axel 2009). In addition, both the total number
228 of spikes across the population (Figure 5D) and the number of spikes evoked per responsive cell
229 (not shown) are only modestly concentration-dependent. Our model therefore shows that piriform
230 circuitry can normalize intensity-scaled input from the olfactory bulb.

To gain insight into how this form of response normalization is implemented, we again simulated responses either without feedforward inhibition or without recurrent excitation and feedback inhibition. Eliminating feedforward inhibition increases both the number of responsive cells (Figure

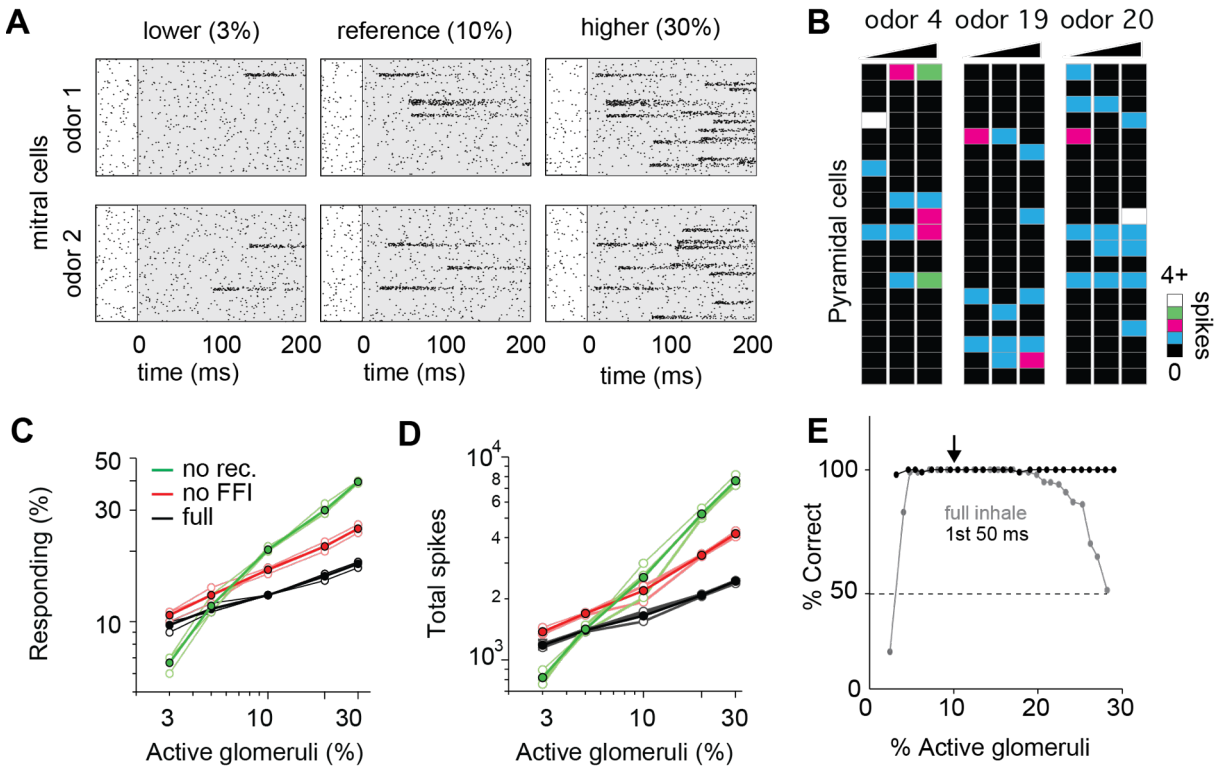

Figure 5. Cortical output is normalized across concentrations.
(A) Mitral cell rasters for 2 odors at 3 different concentrations defined by the fraction of co-active glomeruli. Glomerular onset latencies decrease with concentration allowing more glomeruli to become active over the sniff period. Odors are different from the odors in Figure 1. (B) Single-trial piriform response vectors for single trials over a concentration range corresponding to 3-30% active glomeruli. Note that activity does not dramatically increase despite the 10-fold increase in input. (C) Fraction of activated pyramidal cells at different odor concentrations for the full network (black trace), without FFI (red trace) and without recurrent excitation (green trace) for 4 different odors (open circles, thin lines) and averaged across odors (filled circles, thicker lines). Note that eliminating FFI primarily shifts the number of responsive cells, indicating that FFI is largely subtractive, whereas eliminating recurrent excitation alters the gain of the response. Note also that recurrent excitation amplifies the number of activated cells at low odor concentrations. (D) As in C but for the total number of spikes across the population. (E) Perceptron classifications of an odor at different concentrations on the basis of pyramidal cell activity. Either the transient cortical activity (first 50 ms of the inhalation; black curve) or the activity across the full inhalation (gray curve) was used for both training and testing. Training was solely on the basis of the concentration indicated by the black arrow. The dashed line shows the chance level of classification (50%).

235 5C) and total population spiking (Figure 5D). However, this increase is fairly uniform across con-
236 centrations and removing feedforward inhibition does not substantially change the gain of the re-
237 sponse (i.e. how rapidly these responses vary with input strength; Figure 5C&D), indicating that
238 the effect of feedforward inhibition is largely subtractive. In contrast, eliminating recurrent exci-
239 tation and feedback inhibition destroys concentration invariance by dramatically increasing re-
240 sponse gain, indicating that they implement divisive normalization (Carandini and Heeger 2012).
241 Interestingly, cortical output is decreased at low odor concentrations when recurrent excitatory and
242 feedback inhibition are removed, indicating that recurrent collateral excitation amplifies cortical
243 output in response to weak input (Figure 5C&D).
244
245 Early-activated PCx cells support concentration-invariant odor recognition
246 Because the sequence of glomerular activation latencies is preserved across concentrations, odor
247 representations defined largely by the earliest activated glomeruli could support concentration-
248 invariant odor recognition. We therefore asked whether the cortical odor representation in our
249 model was well-suited to this purpose. Specifically, we next asked if a downstream observer could
250 reliably identify an odor using population spiking, and whether the odor can be recognized when
251 presented at different concentrations. To do this we trained a perceptron to identify a specific odor
252 at one concentration (10% active glomeruli) and then asked how well it could identify that odor
253 presented at different concentrations. We used spike counts over either the full 200 ms inhalation
254 or the first 50 ms as input. Perceptron performance was excellent when trained and tested at a
255 single concentration, indicating that despite considerable trial-to-trial variability, responses to dif-
256 ferent odors can be distinguished reliably (Figure 5E). We then examined classifier performance

when tested on different concentrations without retraining. Performance using the full 200 ms response was generally excellent but fell off at both the lowest and highest concentrations. However, classification using only the early transient response as input was essentially perfect across all tested concentrations. This decoding analysis supports the idea that the earliest cortical response provides an especially good substrate for concentration-invariant odor identification.

Strategies for encoding odor intensity

How is odor intensity represented in PCx? Because both the number of responsive neurons and total spiking are relatively constant across concentrations (Figure 5C-E), spike rate seems unlikely to be used to represent intensity. We therefore examined the dynamics of population spiking in response to odors at different concentrations (Figure 6A). As with the mitral cell activity, cortical response latencies decrease at higher concentrations by a factor of about 2 over a 10-fold increase in input from bulb (Figure 6B), suggesting that a latency code could be used. We also found that the peak of the population response increases by more than a factor of 5 over this range of odor concentration (Figure 6C). Given that total spike output is largely constant, this result indicates that the synchrony of the population piriform response is particularly concentration-dependent. Furthermore, unlike latency, synchrony thus provides an representation of odor intensity that does not require an external reference. The increase in synchrony occurs primarily because activation latencies of the earliest responding glomeruli, which cannot be activated before inhalation onset, compress as odor concentrations increase. causing responses to become more coincident. Thus,

the early peak in the PCx response can be used to rapidly decode both odor identity and concentration.

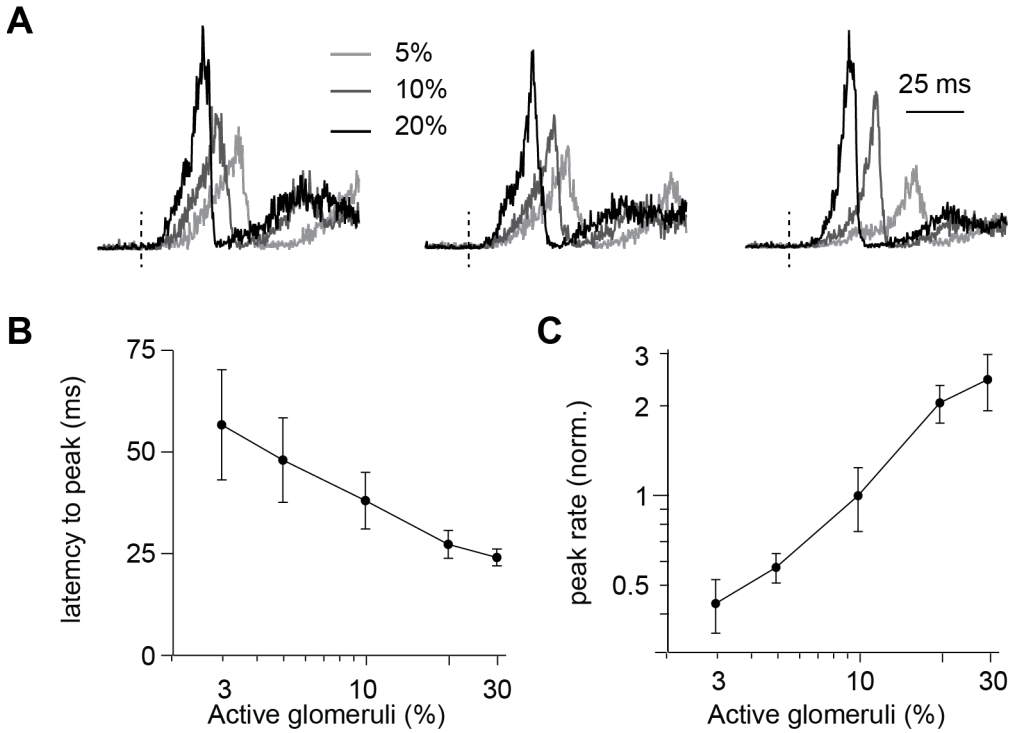

Figure 6. Effect of odor concentration on response timing
(A). Normalized population spike rates for 3 odors at 3 concentrations denoted by percentage of glomeruli responding. Peak responses are higher and occur earlier at higher concentrations. Dashed lines indicate inhalation onset. Average latencies to peak (B) and peak rate (C) vs. number of activated glomeruli.

DISCUSSION

The model we have developed and analyzed provides mechanistic insight into the transformation from an odor code using latency in olfactory bulb to a spatial, ensemble code in the PCx (for an alternative model, see (Sanders et al. 2014)). Individual glomeruli are activated at different latencies after inhalation onset, with glomeruli corresponding to the highest affinity receptors for a given odorant activated earliest. Only a small subset of responsive piriform neurons receives input from many of these early-activated inputs. However, because pyramidal cells are connected via long-range recurrent collateral inputs, these few activated cells provide diffuse excitatory synaptic input across PCx that can bring a larger subset of pyramidal cells that received subthreshold bulb input to threshold. This cascade of cortical activity continues until feedback inhibitory neurons are activated, which then strongly suppresses subsequent cortical spiking. Thus, the earliest activated glomeruli play a dominant role generating PCx odor ensembles. Increasing odor concentration systematically decreases glomerular onset latencies but does not change the sequence in which they are activated. Consequently, a given odor will activate similar ensembles of PCx neurons over a large range of concentrations. In this way, odor identity can be decoded across a wide range of concentrations. Odor concentration, on the other hand, is primarily encoded by the degree of synchrony of the cortical response.

Different odors activate distinct subsets of glomeruli and the number of activated glomeruli increases with odorant concentration (Rubin and Katz 1999, Meister and Bonhoeffer 2001, Spors and Grinvald 2002). However, considerable processing of this input occurs within olfactory bulb so that mitral cells can either be activated or suppressed by odor (Shusterman et al. 2011, Fukunaga et al. 2012, Economo et al. 2016), and normalization within the bulb (Cleland et al. 2011) entails

302 that MTC output scales much less steeply with concentration than the number of activated glomer-
303 uli (Banerjee et al. 2015, Sirotin et al. 2015, Roland et al. 2016). Nevertheless, here we have used
304 a highly simplified olfactory bulb model in which mitral cells are only activated by odor and the
305 number of activated mitral cells increases steeply with concentration. This has allowed us to ex-
306 amine the sufficiency of the cortical circuitry in transforming the temporal bulb representation and
307 normalizing output. Adding suppressed responses would slightly decrease the peak and deepen the
308 subsequent trough of the cortical response (Figure 2), and some normalization across concentra-
309 tions within the bulb would result in even less concentration-dependence in PCx (Figure 5). We
310 have also not attempted to separately model mitral and tufted cell responses. In fact, odor-evoked
311 responses in tufted cells occur reliably with short latencies whereas mitral cells, whose activity we
312 simulate, fire slightly later and with latencies that decrease with concentration (Fukunaga et al.
313 2012). This would be expected to produce a somewhat biphasic bulb and cortical response, with a
314 more rapid and concentration-invariant component and a later, concentration-dependent compo-
315 nent. Recent simultaneous bulb-PCx recordings are consistent with these predictions (Bolding and
316 Franks, *submitted*). We have also not attempted to distinguish here between different subclasses
317 of principal neurons (e.g. semilunar cells versus superficial pyramidal cells) or inhibitory inter-
318 neurons (e.g. somatostatin versus parvalbumiun-expressing GABAergic interneurons) in this
319 model. No doubt incorporating these distinctions will alter network behavior somewhat but the
320 overall dynamics of this network and general conclusions that we draw here are expected to be
321 robust, and therefore these refinements are appropriate for future, updated versions of the model
322 but beyond the scope of this project.
323

Our model predicts considerable trial-to-trial variability for same-odor responses and very low correlations between responses to different odors. Both these values are lower than recent experimental measures obtained by in vivo imaging (Roland et al *submitted*) or extracellular spiking (Bolding & Franks, *submitted*). Responses correlations to different odors in the model PCx are close to zero, which is expected because bulb inputs are random and cells receive no other sources of excitation. However, what underlies the high trial-to-trial variability? In our model, mitral cell spiking is governed by a Poisson process. Because inputs from OB to PCx are randomly assigned, this stochasticity is reflected in the input to individual pyramidal cells from mitral cells that are innervated by the same glomerulus (i.e. sister mitral cells). However, sister mitral cells are electrically coupled by gap junctions in their apical dendrites (Christie et al. 2005) and spiking in pairs of sister mitral cells can be highly correlated (Schoppa 2006). Correlated spiking in sister mitral cells would more synchronously innervate the set of piriform neurons receiving input from an activated glomerulus. The effect of this electrical coupling could be determined directly by examining the reliability of cortical odor responses in mice lacking connexin-36. In addition, recurrent connections between pyramidal cells in the model are also random. However, these synapses are plastic and are thought to provide a substrate for forming assemblies of similarly responsive neurons (Haberly 2001, Wilson and Sullivan 2011). Such assemblies could help complete ensembles of cells that are regularly co-activated, thereby decreasing trial-to-trial variability. Thus, correlated spiking in sister mitral cells and specific recurrent connectivity between cortical pyramidal cells may increase the fidelity of cortical odor responses.

Piriform cortex neurons are interconnected via a diffuse, long-range recurrent collateral excitatory plexus that also recruits strong and scaled feedback inhibition (Johnson et al. 2000, Franks et al.

2011, Suzuki and Bekkers 2012). Our model shows how this circuitry amplifies the impact of the earliest responsive glomeruli and discounts the impact of glomeruli that respond later. Why would a sensory system discard so much information about the stimulus? To represent a large extent of potential odorant space, the olfactory system employs a huge number of distinct odorant receptors that are each highly selective for a small fraction of potential odorants. Thus, any given odorant will strongly activate only a few, optimally-tuned receptors, while many other receptors will be moderately or weakly activated if they receive input from sensory neurons expressing receptors with lower affinity for the odor, especially at high concentrations. However, the few odorant receptors with the highest affinities to a given odorant will always be more strongly activated, and therefore their associated glomeruli and MTCs will be activated earlier than those receiving input from lower affinity receptors, regardless of odorant concentration. By defining odors according to the earliest responding glomeruli, the olfactory system retains the specificity of the odor representation and discards spurious information provided by non-specific receptor activations.

360 **MATERIALS AND METHODS**

361 **Modeling**

362 Model olfactory bulb

363 The model bulb includes 900 glomeruli with 25 model mitral cells assigned to each glumerulus.
364 Odor concentrations are defined by specifying a fraction *f* of glomeruli that respond to an odor at
365 that concentration. Then, for every odor, each glomerulus is assigned a reference onset latency
366 between 0 to 200 ms. At our reference concentration 10% of the glomeruli have onset latencies
367 <200 ms. The actual glomerular onset latencies for a given concentration are then obtained by
368 dividing the set of reference latencies by *f*. Glomeruli with latencies longer than the duration of
369 the inhalation are not activated. Mitral cell spiking is modeled as a Poisson process that generates
370 action potentials at specified rates; baseline spike rate is 1-2 Hz, which steps to 100 Hz when a
371 glomerulus is activated and then decays back to baseline with a time constant of 50 ms. This Pois-
372 son-generated mitral cell spiking introduces stochasticity into our olfactory bulb model.

373

374 Model piriform architecture and connectivity

375 The piriform model includes three types of model cells: 10,000 excitatory pyramidal cells, 1,225
376 feedforward inhibitory cells (FFI), and 1,225 feedback inhibitory cells (FBI). The model pyramidal
377 cells and FBIs are assigned to locations on a two-layer grid. Pyramidal cells and FBIs are uni-
378 formly spread over the grid on their respective layers. Each pyramidal cell receives an input from
379 1000 random other pyramidal cells and from 50 FFIs, both independent of location. Each pyram-
380 idal cell receives local input from the closest (on average) 12 FBIs. Each FBI receives input from
381 1,000 randomly chosen pyramidal cells and 8 (on average) closest FBIs. Each FFI receives input

from 50 other randomly chosen FFIs. Each mitral cell sends input to 25 random cells (either pyramidal cells or FFIs) in the pirifom. As a result, each pyramidal and FFI cell receives input from approximately 50 random mitral cells.

Piriform Dynamics

The piriform model cells are modeled as leaky integrate-and-fire neurons with the membrane potential V_i of model piriform cell following the dynamical equation

$$_m \frac{dV_i}{dt} = (V_r \quad V_i) + I_{i,ex} \quad I_{i,in} + I_{i,ext}$$

Here $_m = 15\text{ms}$ is the membrane time constant, $V_r = \quad 65\text{mV}$ is the resting potential and $I_{i,ex}$, $I_{i,in}$ and $I_{i,ext}$ are the excitatory, inhibitory and external synaptic currents (of cell) respectively. We have absorbed a factor of the membrane resistance into the definition of the input currents so they are measured in the same units as the membrane potential (mV). When the membrane potential V reaches the firing threshold $V_{th} = \quad 50\text{mV}$ the neuron fires an action potential and the membrane potential is reset to the resting value V_r, where it remains for a refractory period $_{ref} = 1\text{ms}$.

The minimum allowed value for the membrane potential is $V_{\min} = \quad 75\text{mV}$. From this value the membrane potential can only rise, following the dynamics, it cannot be decreased. Each action potential fired by a neuron induces an instantaneous jump in the current of all its postsynaptic targets by an amount proportional to the appropriate synaptic weight. Action potentials in FFIs and FBIs affect the inhibitory current of their postsynaptic target neurons while action potentials

in the pyrmidal cells affect the excitatory current of their postsynaptic targets. Mitral cell spikes also contribute to the excitatory current of the appropriate postsynaptic cells.

The inhibitory and excitatory currents dynamics are described by

$$\tau_{ex}\frac{dI_{i,ex}}{dt} = -I_{i,ex} + \tau_{ex}\sum_{j_{Ex}\to i} S_{ij,ex}\sum_{k}^{t_k^j<t}\delta(t_k^j - t) + \tau_{ex}\sum_{j_{Mitral}\to i} S_{ij,Mitral}\sum_{k}^{t_k^j<t}\delta(t_k^j - t)$$

$$_{in}\frac{dI_{i,in}}{dt} = \quad I_{i,in} + \quad _{in}\quad _{j_{Ff;Fb}}\quad S_{ij,in}\quad _{i}\quad _{k}^{t_k^j<t}\quad (t_k^j \quad t)$$

The synaptic time constants are given by $_{ex} = 20\text{ms}$ and $_{in} = 10\text{ms}$. The excitatory current combines two components, AMPA and NMDA, into a single current. Because the NMDA synapses are relatively slow and AMPA relatively fast, we choose the time constant of this composite current in an intermediate range between these two extremes. In each term that includes summation over contributions to the current, the first sum runs over all neurons that are presynaptic to neuron and that contributes to the specified current. The second sum runs over all the times t_k^j of spikes produced by presynaptic neuron prior to time , indexed by . The synaptic weight between presynaptic Ex cell and postsynaptic Ex or Fb cell is given by $S_{ij}^{Ex\quad Ex} = 0.25\text{mV}$ and $S_{ij}^{Ex\quad Fb} = 1\text{mV}$ respectively. The synaptic weight between presynaptic Mitral cell and postsynaptic pyramidal or FFI is given by $S_{ij}^{Mitral\to Ex,Ff} = 10\text{mV}$. The synaptic weight between presynaptic FFI and postsynaptic pyramidal or FFI cell is given by $S_{ij}^{Ff\to Ex,Ff} = 10\text{mV}$. The synaptic weight between presynaptic FBI and postsynaptic pyramidal or FBI has the same strength, $S_{ij}^{Fb\to Ex,Fb} = 10\text{mV}$.

It is useful to describe the strengths of the different synapses we have discussed in terms of unitary PSP sizes rather than using the S parameters given above. Using the constants we have given and the synaptic and membrane dynamics, we calculated peak EPSPs and IPSPs. All inhibitory inputs create IPSPs at the postsynaptic cell with a peak deflection of . EPSPs from mitral cell produce . The EPSP for input from pyramidal to pyramidal or to FBI cell has or respectively.

The external input is constant in time but depend on cell identity. For all pyramidal cells it is given by

$$I_{i,ext} = \quad 0.5 + I_{rand}(i)$$

where $I_{rand}(i)$ is a random number generated from a Gaussian distribution with zero mean and standard deviation . The external input for all other cells is zero.

<u>Pyramidal cell population activity vectors</u>

To analyze cortical responses, we define an activity vector . Each component of this vector, , is the number of spikes generated by pyramidal neuron . Because we are interested in odor responses, we start to count spikes at the beginning of the inhalation. The spikes count continues across the full inhale, or stops after 50 ms in cases when we are interested in the initial response only. The activity maps in the figures are a visual representation of the activity vectors created by reshaping the vectors and assigning a color on the basis of their component values.

<u>Activity correlation coefficients</u>

To compute the correlation between two cortical responses on two different trials, we calculate the correlation coefficient between the corresponding activity vectors, $\bar{r}_1$, $\bar{r}_2$,

$$c = \frac{\sum_{i=1}^{N}\left(r_{1,i} - <\bar{r}_1>\right)\left(r_{2,i} - <\bar{r}_2>\right)}{\sqrt{\sum_{i=1}^{N}\left(r_{1,i} - <\bar{r}_1>\right)^2}\sqrt{\sum_{i=1}^{N}\left(r_{2,i} - <\bar{r}_2>\right)^2}}$$

with $N = 10{,}000$ the number of pyramidal cells and $<\bar{r}>$ the average value of the entries of $\bar{r}$.

<u>The perceptron</u>

We use a perceptron, defined by a weights vector $\overline{w}$, to classify odor responses to odors on the basis of the activity vectors explained above. Our goal is to train the perceptron such that trials involving a chosen target odor are distinguished from trials using other odors. Because we generate odors randomly and all model mitral cells behave similarly, the results are independent of the choice of target odor. Distinguishing the activity for a target odor from all other activity patterns means that we wish to find $\overline{w}$ such that trials with a target odor have $\overline{w} \cdot \bar{r} > 0$ and trials with other odors have $\overline{w} \cdot \bar{r} < 0$. Such a $\overline{w}$ only exists if trials using the target odor are linearly separable from trials using other odors. If such a perceptron weight vector exists, we know that pyramidal cell activity in response to a specific odor are inherently distinguishable from activity for other odors. Furthermore, because the activity vectors we use do not contain temporal information, we know that the discrimination relies solely on the identity of the active pyramidal cells, these are the pyramidal cell ensembles, and their firing rates.

During training, 100 odors were presented at a specific concentration (10% activated glomeruli) over a total of 600 trials. Odor 1 was chosen as the target, and the trials alternated between this target odor and all odors. Thus, odor 1 was presented 303 times and every other odor 3 time. On

every trial, the quantity $\overline{w} \cdot \bar{r}$ was calculated, with $\bar{r}$ the activity vector for that trial and $\overline{w}$ the current perceptron weight vector. Initially, $\overline{w}$ was zero. If classification was correct, meaning $\overline{w} \cdot \bar{r} > 0$ for the target odor trial or $\overline{w} \cdot \bar{r} < 0$ for other odors, $\overline{w}$ was left unchanged. Otherwise $\overline{w}$ was updated to $\overline{w} + \bar{r}$ or $\overline{w} - \bar{r}$ for trials of odor 1 or for other odors, respectively. The entire training procedure was repeated twice, once with activity vectors that included spikes counts around the peak of the piriform activity (the first $50ms$ of inhale) and once using spikes counts from the entire inhalation.

To test the perceptron, each odor was presented at many concentrations (even though training was done only for a single fixed concentration). For the target odor 100 trials were tested at each concentration (30 different concentrations ranging between 3% activated glomeruli and 30% activated glomeruli). Each trial that gave $\overline{w} \cdot \bar{r} > 0$ was considered a correct classification. For each concentration, the percentage of trials that were correctly classified was calculated. Trials with non-target odors were tested as well, one trial for each odor at each concentration. All the non-target odors were correctly classified as not target ($\overline{w} \cdot \bar{r} < 0$) across all concentrations. The testing procedure was done using both the peak and full activity vectors, with the corresponding perceptron weight vectors.

483 **REFERENCES**

484 Abraham, N. M., H. Spors, A. Carleton, T. W. Margrie, T. Kuner and A. T. Schaefer (2004).
485 "Maintaining accuracy at the expense of speed: stimulus similarity defines odor discrimination
486 time in mice." Neuron **44**(5): 865-876.

487 Apicella, A., Q. Yuan, M. Scanziani and J. S. Isaacson (2010). "Pyramidal Cells in Piriform Cortex
488 Receive Convergent Input from Distinct Olfactory Bulb Glomeruli." Journal of Neuroscience
489 **30**(42): 14255-14260.

490 Banerjee, A., F. Marbach, F. Anselmi, M. S. Koh, M. B. Davis, P. Garcia da Silva, K. Delevich,
491 H. K. Oyibo, P. Gupta, B. Li and D. F. Albeanu (2015). "An Interglomerular Circuit Gates
492 Glomerular Output and Implements Gain Control in the Mouse Olfactory Bulb." Neuron **87**(1):
493 193-207.

494 Bathellier, B., D. L. Buhl, R. Accolla and A. Carleton (2008). "Dynamic ensemble odor coding in
495 the mammalian olfactory bulb: sensory information at different timescales." Neuron **57**(4): 586-
496 598.

497 Bozza, T., J. P. McGann, P. Mombaerts and M. Wachowiak (2004). "In vivo imaging of neuronal
498 activity by targeted expression of a genetically encoded probe in the mouse." Neuron **42**(1): 9-21.

499 Cang, J. and J. S. Isaacson (2003). "In vivo whole-cell recording of odor-evoked synaptic
500 transmission in the rat olfactory bulb." J Neurosci **23**(10): 4108-4116.

501 Carandini, M. and D. J. Heeger (2012). "Normalization as a canonical neural computation." Nat
502 Rev Neurosci **13**(1): 51-62.

503 Carey, R. M., J. V. Verhagen, D. W. Wesson, N. Pirez and M. Wachowiak (2009). "Temporal
504 structure of receptor neuron input to the olfactory bulb imaged in behaving rats." J Neurophysiol
505 **101**(2): 1073-1088.

506 Christie, J. M., C. Bark, S. G. Hormuzdi, I. Helbig, H. Monyer and G. L. Westbrook (2005).
507 "Connexin36 mediates spike synchrony in olfactory bulb glomeruli." Neuron **46**(5): 761-772.
508 Cleland, T. A., S. Y. Chen, K. W. Hozer, H. N. Ukatu, K. J. Wong and F. Zheng (2011).
509 "Sequential mechanisms underlying concentration invariance in biological olfaction." Front
510 Neuroeng **4**: 21.
511 Cury, K. M. and N. Uchida (2010). "Robust odor coding via inhalation-coupled transient activity
512 in the mammalian olfactory bulb." Neuron **68**(3): 570-585.
513 Davison, I. G. and M. D. Ehlers (2011). "Neural Circuit Mechanisms for Pattern Detection and
514 Feature Combination in Olfactory Cortex." Neuron **70**(1): 82-94.
515 Economo, M. N., K. R. Hansen and M. Wachowiak (2016). "Control of Mitral/Tufted Cell Output
516 by Selective Inhibition among Olfactory Bulb Glomeruli." Neuron **91**(2): 397-411.
517 Franks, K. M. and J. S. Isaacson (2006). "Strong single-fiber sensory inputs to olfactory cortex:
518 implications for olfactory coding." Neuron **49**(3): 357-363.
519 Franks, K. M., M. J. Russo, D. L. Sosulski, A. A. Mulligan, S. A. Siegelbaum and R. Axel (2011).
520 "Recurrent circuitry dynamically shapes the activation of piriform cortex." Neuron **72**(1): 49-56.
521 Fukunaga, I., M. Berning, M. Kollo, A. Schmaltz and A. T. Schaefer (2012). "Two distinct
522 channels of olfactory bulb output." Neuron **75**(2): 320-329.
523 Ghosh, S., S. D. Larson, H. Hefzi, Z. Marnoy, T. Cutforth, K. Dokka and K. K. Baldwin (2011).
524 "Sensory maps in the olfactory cortex defined by long-range viral tracing of single neurons."
525 Nature **472**(7342): 217-220.
526 Gschwend, O., J. Beroud and A. Carleton (2012). "Encoding odorant identity by spiking packets
527 of rate-invariant neurons in awake mice." PLoS One **7**(1): e30155.

528 Haberly, L. B. (2001). "Parallel-distributed processing in olfactory cortex: new insights from
529 morphological and physiological analysis of neuronal circuitry." Chem Senses **26**(5): 551-576.
530 Haddad, R., A. Lanjuin, L. Madisen, H. Zeng, V. N. Murthy and N. Uchida (2013). "Olfactory
531 cortical neurons read out a relative time code in the olfactory bulb." Nat Neurosci **16**(7): 949-957.
532 Homma, R., L. B. Cohen, E. K. Kosmidis and S. L. Youngentob (2009). "Perceptual stability
533 during dramatic changes in olfactory bulb activation maps and dramatic declines in activation
534 amplitudes." Eur J Neurosci **29**(5): 1027-1034.
535 Hopfield, J. J. (1995). "Pattern recognition computation using action potential timing for stimulus
536 representation." Nature **376**(6535): 33-36.
537 Illig, K. R. and L. B. Haberly (2003). "Odor-evoked activity is spatially distributed in piriform
538 cortex." J Comp Neurol **457**(4): 361-373.
539 Johnson, D. M. G., K. R. Illig, M. Behan and L. B. Haberly (2000). "New features of connectivity
540 in piriform cortex visualized by intracellular injection of pyramidal cells suggest that "primary"
541 olfactory cortex functions like "association" cortex in other sensory systems." Journal of
542 Neuroscience **20**(18): 6974-6982.
543 Junek, S., E. Kludt, F. Wolf and D. Schild (2010). "Olfactory coding with patterns of response
544 latencies." Neuron **67**(5): 872-884.
545 Krone, D., M. Mannel, E. Pauli and T. Hummel (2001). "Qualitative and quantitative olfactometric
546 evaluation of different concentrations of ethanol peppermint oil solutions." Phytother Res **15**(2):
547 135-138.
548 Laing, D. G., P. K. Legha, A. L. Jinks and I. Hutchinson (2003). "Relationship between molecular
549 structure, concentration and odor qualities of oxygenated aliphatic molecules." Chem Senses
550 **28**(1): 57-69.

Large, A. M., N. W. Vogler, S. Mielo and A. M. Oswald (2016). "Balanced feedforward inhibition and dominant recurrent inhibition in olfactory cortex." Proc Natl Acad Sci U S A **113**(8): 2276-2281.

Luna, V. M. and N. E. Schoppa (2008). "GABAergic circuits control input-spike coupling in the piriform cortex." Journal of Neuroscience **28**(35): 8851-8859.

Margrie, T. W. and A. T. Schaefer (2003). "Theta oscillation coupled spike latencies yield computational vigour in a mammalian sensory system." J Physiol **546**(Pt 2): 363-374.

Meister, M. and T. Bonhoeffer (2001). "Tuning and topography in an odor map on the rat olfactory bulb." J Neurosci **21**(4): 1351-1360.

Miura, K., Z. F. Mainen and N. Uchida (2012). "Odor representations in olfactory cortex: distributed rate coding and decorrelated population activity." Neuron **74**(6): 1087-1098.

Miyamichi, K., F. Amat, F. Moussavi, C. Wang, I. Wickersham, N. R. Wall, H. Taniguchi, B. Tasic, Z. J. Huang, Z. G. He, E. M. Callaway, M. A. Horowitz and L. Q. Luo (2011). "Cortical representations of olfactory input by trans-synaptic tracing." Nature **472**(7342): 191-196.

Poo, C. and J. S. Isaacson (2009). "Odor Representations in Olfactory Cortex: "Sparse" Coding, Global Inhibition, and Oscillations." Neuron **62**(6): 850-861.

Poo, C. and J. S. Isaacson (2011). "A major role ofor intracortical circuits in the strength and tuning of odor-evoked excitation in olfactory cortex." Neuron **72**(1): 41-48.

Rennaker, R. L., C. F. Chen, A. M. Ruyle, A. M. Sloan and D. A. Wilson (2007). "Spatial and temporal distribution of odorant-evoked activity in the piriform cortex." J Neurosci **27**(7): 1534-1542.

Rinberg, D., A. Koulakov and A. Gelperin (2006). "Speed-accuracy tradeoff in olfaction." Neuron **51**(3): 351-358.

Roland, B., R. Jordan, D. L. Sosulski, A. Diodato, I. Fukunaga, I. Wickersham, K. M. Franks, A. T. Schaefer and A. Fleischmann (2016). "Massive normalization of olfactory bulb output in mice with a 'monoclonal nose'." Elife **5**.

Rubin, B. D. and L. C. Katz (1999). "Optical imaging of odorant representations in the mammalian olfactory bulb." Neuron **23**(3): 499-511.

Sanders, H., B. E. Kolterman, R. Shusterman, D. Rinberg, A. Koulakov and J. Lisman (2014). "A network that performs brute-force conversion of a temporal sequence to a spatial pattern: relevance to odor recognition." Front Comput Neurosci **8**: 108.

Schaefer, A. T. and T. W. Margrie (2007). "Spatiotemporal representations in the olfactory system." Trends Neurosci **30**(3): 92-100.

Schaefer, A. T. and T. W. Margrie (2012). "Psychophysical properties of odor processing can be quantitatively described by relative action potential latency patterns in mitral and tufted cells." Front Syst Neurosci **6**: 30.

Schoppa, N. E. (2006). "Synchronization of olfactory bulb mitral cells by precisely timed inhibitory inputs." Neuron **49**(2): 271-283.

Shusterman, R., M. C. Smear, A. A. Koulakov and D. Rinberg (2011). "Precise olfactory responses tile the sniff cycle." Nat Neurosci **14**(8): 1039-1044.

Sirotin, Y. B., R. Shusterman and D. Rinberg (2015). "Neural Coding of Perceived Odor Intensity." eNeuro **2**(6).

Sosulski, D. L., M. L. Bloom, T. Cutforth, R. Axel and S. R. Datta (2011). "Distinct representations of olfactory information in different cortical centres." Nature **472**(7342): 213-216.

Spors, H. and A. Grinvald (2002). "Spatio-temporal dynamics of odor representations in the mammalian olfactory bulb." Neuron **34**(2): 301-315.

Spors, H., M. Wachowiak, L. B. Cohen and R. W. Friedrich (2006). "Temporal dynamics and latency patterns of receptor neuron input to the olfactory bulb." J Neurosci **26**(4): 1247-1259.

Stettler, D. D. and R. Axel (2009). "Representations of Odor in the Piriform Cortex." Neuron **63**(6): 854-864.

Stokes, C. C. A. and J. S. Isaacson (2010). "From Dendrite to Soma: Dynamic Routing of Inhibition by Complementary Interneuron Microcircuits in Olfactory Cortex." Neuron **67**(3): 452-465.

Suzuki, N. and J. M. Bekkers (2006). "Neural coding by two classes of principal cells in the mouse piriform cortex." J Neurosci **26**(46): 11938-11947.

Suzuki, N. and J. M. Bekkers (2012). "Microcircuits mediating feedforward and feedback synaptic inhibition in the piriform cortex." J Neurosci **32**(3): 919-931.

Uchida, N. and Z. F. Mainen (2003). "Speed and accuracy of olfactory discrimination in the rat." Nat Neurosci **6**(11): 1224-1229.

Uchida, N., C. Poo and R. Haddad (2014). "Coding and transformations in the olfactory system." Annu Rev Neurosci **37**: 363-385.

Wesson, D. W., R. M. Carey, J. V. Verhagen and M. Wachowiak (2008). "Rapid encoding and perception of novel odors in the rat." PLoS Biol **6**(4): e82.

Wilson, C., G. Serrano, A. Koulakov and D. Rinberg (2015). Primacy coding of odor identity across concentrations. Society for Neuroscience. **229.01**.

Wilson, D. A. and R. M. Sullivan (2011). "Cortical processing of odor objects." Neuron **72**(4): 506-519.

Wilson, R. I. and Z. F. Mainen (2006). "Early events in olfactory processing." Annu Rev Neurosci **29**: 163-201.

Zhan, C. and M. Luo (2010). "Diverse patterns of odor representation by neurons in the anterior piriform cortex of awake mice." J Neurosci **30**(49): 16662-16672.

624 **FIGURE LEGENDS**

625 **Figure 1. Odors activate distributed ensembles of PCx neurons.**

626 (A) Raster plots showing spiking of 1,000 mitral cells (out of 22,500 total; 25 mitral cells/glomer-
627 ulus, 40 glomeruli shown) in response to 3 different odors. Each row represents a single mitral cell
628 and all mitral cells belonging to each glomerulus are clustered. Tick marks indicate spike times.
629 Inhalation begins at 0 ms and is indicated by the grey shaded region. The red curve shows the
630 cumulative number of glomeruli activated across the sniff, and the blue curve is the firing rate
631 averaged across all mitral cells.

632 (B) Schematic of the piriform cortex model.

633 (C) Voltage traces for three sequential sniffs in 4 model pyramidal cells. Time of inhalation is
634 indicated by the dashed line.

635 (D) Single-trial population activity map for all 10,000 pyramidal cells. Each pixel represents a
636 single cell, and pixel color indicates the number of spikes fired during the 200 ms inhalation. Ap-
637 proximately 13% of cells fired at least 1 action potential, with activated cells randomly distributed
638 across the cortex.

639 (E) Response vectors shown for 20 cells in response to different odors presented on 4 sequential
640 trials. Spiking levels are low for no-odor controls. Note the trial-to-trial variability and that indi-
641 vidual cells can be activated by different odors.

642

643 **Supplementary Figure 1. Modeling odor responses in olfactory bulb**

644 (A) Raster for all 22,500 mitral cells for one odor trial. Grey shading indicates inhalation phase.
645 Inset shows expanded view of 1,000 mitral cells belonging to 40 different glomeruli.

646 (B) Raster showing trial-to-trial variability for a single activated glomerulus. Each box represents
647 a different sister mitral cell, with trials 1-4 represented by the lines within each box.
648
649 **Figure 2. Evolution of a cortical odor response.**
650 (A) Raster for a single sniff showing spiking activity of a subset of mitral cells (2,250 out of
651 22,500), all 1,225 feedforward interneurons (FFIs), all 10,000 pyramidal cells, and all 1,225 feed-
652 forward interneurons (FBIs). Spiking rate for the population of pyramidal cells is shown at the
653 bottom (average of 6 trials). Note that the earliest activated glomeruli initiate a cascade of pyram-
654 idal cell spiking that peaks after ~50 ms and is abruptly truncated by synchronous spiking of FBIs.
655 (B) Single-trial voltage traces (black) for 3 pyramidal cells in response to the same odor. Inhalation
656 onset is indicated by the dashed line. The red traces show the bulb input and the green traces the
657 recurrent input received by each cell. Cell 1 receives strong bulb input and spikes soon after odor
658 presentation. Cell 2 receives subthreshold input from the bulb and only spikes after receiving
659 addition recurrent input from other pyramidal cells. Cell 3 receives no early odor-evoked input
660 from the bulb, and its recurrent input is subthreshold, so it does not spike over the time period
661 shown.
662
663 **Figure 3. Distinct roles for different inputs in shaping ensemble response.**
664 (A-D) Raster plots for presentations of the same odor using different circuit configurations. The
665 percentages of active pyramidal cells are shown in the insets.
666 (A) As in Figure 2A.

667 (B) Network activity when pyramidal cells get excitatory input from mitral cells but without FFI,
668 recurrent excitation or FBI. Pyramidal cell spiking tracks mitral cell input. Population rate for the
669 full network is shown in grey for comparison.
670 (C) Network activity after eliminating excitatory input to FFIs. Note that sustained FBI spiking
671 increases without FFI, resulting in roughly constant levels of sustained spiking in pyramidal cells.
672 (D) Network activity with no recurrent excitation onto either other pyramidal cells or FBIs. The
673 transient activity peak seen in A-D is absent, and sustained activity is slightly higher.
674 (E) Population rate plots for 3 different odors with the full network (black trace), no FFI (red trace)
675 or no recurrent excitation/FBI (green trace). Insets expand the period around inhalation. Note the
676 population spiking is higher and peaks slightly earlier without FFI, and that responses are slow
677 without recurrent excitation. All population spike rate plots are averaged over 6 trials.
678
679 **Figure 4. Earliest-active glomeruli define the cortical response.**
680 (A) Normalized population spike rates (black) in response to an odor during the sniff cycle shown
681 in grey. The red curve shows the cumulative number of glomeruli activated across the sniff. Note
682 that population spiking peaks after only a small subset of glomeruli have been activated.
683 (B) Normalized population spike rates for one odor for the full network (black trace), without FFI
684 (red trace) and without recurrent excitation (green trace). Grey trace shows the cumulative number
685 of activated glomeruli.
686 (C) Fraction of peak population spike rate as a function of the cumulative number of activated
687 glomeruli for 6 different odors. These curves indicate the central role recurrent excitation plays in
688 amplifying the impact of early-responsive glomeruli.

(D) Average correlation coefficients for repeated same-odor trials and pairs of different-odor trials measured over the full 200 ms inhalation.

(E) As in D but measured over the first 50 ms after inhalation onset.

(F) Ratios of correlations for same- vs. different-odor trials measured over the full sniff (grey bar on left) and over the first 50 ms (black bar on right).

Figure 5. Cortical output is normalized across concentrations.

(A) Mitral cell rasters for 2 odors at 3 different concentrations defined by the fraction of co-active glomeruli. Glomerular onset latencies decrease with concentration allowing more glomeruli to become active over the sniff period. Odors are different from the odors in Figure 1.

(B) Single-trial piriform response vectors for single trials over a concentration range corresponding to 3-30% active glomeruli. Note that activity does not dramatically increase despite the 10-fold increase in input.

(C) Fraction of activated pyramidal cells at different odor concentrations for the full network (black trace), without FFI (red trace) and without recurrent excitation (green trace) for 4 different odors (open circles, thin lines) and averaged across odors (filled circles, thicker lines). Note that eliminating FFI primarily shifts the number of responsive cells, indicating that FFI is largely subtractive, whereas eliminating recurrent excitation alters the gain of the response. Note also that recurrent excitation amplifies the number of activated cells at low odor concentrations.

(D) As in C but for the total number of spikes across the population.

(E) Perceptron classifications of an odor at different concentrations on the basis of pyramidal cell activity. Either the transient cortical activity (first 50 ms of the inhalation; black curve) or the activity across the full inhalation (gray curve) was used for both training and testing. Training was

712 solely on the basis of the concentration indicated by the black arrow. The dashed line shows the
713 chance level of classification (50%).
714
715 **Figure 6. Effect of odor concentration on response timing**
716 (A). Normalized population spike rates for 3 odors at 3 concentrations denoted by percentage of
717 glomeruli responding. Peak responses are higher and occur earlier at higher concentrations.
718 Dashed lines indicate inhalation onset.
719 Average latencies to peak (B) and peak rate (C) vs. number of activated glomeruli.
720